Multiaperture planar waveguide spectrometer formed by arrayed Mach-Zehnder interferometers

Mirosław Florjańczyk[1, 2 *], Pavel Cheben[2], Siegfried Janz[2], Alan Scott[3], Brian Solheim[1], and Dan-Xia Xu[2]

[1]*CRESS Space Instrumentation Laboratory, York University, Toronto, Ontario, M3J 1P3, Canada*
[2]*Institute for Microstructural Sciences, National Research Council Canada, Ottawa, Ontario, K1A 0R6, Canada*
[3]*COM DEV Ltd., Kanata, Ontario, K2K 3J1, Canada*
**Corresponding author: m.florjanczyk@osa.org*

Abstract: Concept, theory and simulations of a new type of waveguide device, a multiaperture Fourier-transform planar waveguide spectrometer, are presented. The spectrometer is formed by an array of Mach-Zehnder interferometers generating a wavelength dependent spatial fringe pattern at the array output. The input light spectrum is calculated using a discrete Fourier transformation of the output spatial fringes. The multiaperture input significantly increases the optical throughput (*étendue*) compared to conventional single input spectrometers. Design rules for the arrayed spectrometer are deduced from performance specifications such as wavelength range and spectral resolution. A design example with spectral resolution 0.025 nm and range 2.5 nm is presented, where the optical throughput is increased by a factor of 200 compared to a single input device.

OCIS codes: (120.6200) Spectrometers and spectroscopic instrumentation; (230.7390) Waveguides, planar; (300.6300) Spectroscopy, Fourier transform

References and links

1. P. Cheben, "Wavelength dispersive planar waveguide devices: Echelle gratings and arrayed waveguide gratings," in *Optical Waveguides: From Theory to Applied Technologies*, M. L. Calvo and V. Laksminarayanan, eds. (CRC Press, London, 2007).
2. P. Cheben, J. H. Schmid, A. Delâge, A. Densmore, S. Janz, B. Lamontagne, J. Lapointe, E. Post, P. Waldron, and D.-X. Xu, "A high-resolution silicon-on-insulator arrayed waveguide grating microspectrometer with submicrometer aperture waveguides," Opt. Express **15**, 2299-2306 (2007).
3. P. Jacquinot, "The luminosity of spectrometers with prisms, gratings, or Fabry-Perot etalons," J. Opt. Soc. Am. **44**, 761-765 (1954).
4. P. B. Fellgett, "The theory of infra-red sensitivities and its application to investigations of stellar radiation in the near infra-red," Ph.D. dissertation (University of Cambridge, Cambridge, UK, 1951).
5. P. Fellgett, "A propos de la théorie du spectromètre interférentiel multiplex," J. Phys. Radium **19**, 187-191 (1958).
6. M.-L. Junttila, J. Kauppinen, and E. Ikonen, "Performance limits of stationary Fourier spectrometers," J. Opt. Soc. Am. A **8**, 1457-1462 (1991).
7. J. Harlander, R. J. Reynolds, and F. L. Roesler, "Spatial heterodyne spectroscopy for the exploration of diffuse interstellar emission lines at far-ultraviolet wavelengths," Astrophys. J. **396**, 730-740 (1992).
8. P. Cheben, I. Powell, S. Janz, and D.-X. Xu, "Wavelength-dispersive device based on a Fourier-transform Michelson-type arrayed waveguide grating," Opt. Lett. **30**, 1824-1826 (2005).
9. J. A. Rodrigo, P. Cheben, T. Alieva, M. L. Calvo, M. Florjańczyk, S. Janz , A. Scott , B. Solheim , D.-X. Xu, and A. Delâge, "Fresnel diffraction effects in Fourier-transform arrayed waveguide grating spectrometer," Opt. Express **15**, 16431-16441 (2007).
10. M. Florjańczyk, P. Cheben, S. Janz, A. Scott, B. Solheim, and D.-X. Xu, "Planar waveguide spatial heterodyne spectrometer," Proc. SPIE **6796**, 67963J-1 (2007).
11. I. Powell and P. Cheben, "Modeling of the generic spatial heterodyne spectrometer and comparison with conventional spectrometer," Appl. Opt. **45**, 9079-9086 (2006).
12. F. C. Garcia, L. Vogelaar, and R. Kashyap, "Poling of a channel waveguide," Opt. Express **11**, 3041-3047 (2003).

#89497 - $15.00 USD Received 7 Nov 2007; revised 17 Dec 2007; accepted 18 Dec 2007; published 19 Dec 2007

13. W. H. Steel, "Symbols Units Nomenclature: Luminosity, throughput, or etendue? Further comments," Appl. Opt. **14**, 252-253 (1974).
14. Ch. K. Madsen and J. H. Zhao, *Optical Filter Design and Analysis: A Signal Processing Approach* (Wiley-Interscience, New York, 1999).
15. J. Chamberlain, *The Principles of Interferometric Spectroscopy* (Wiley-Interscience, Chichester, UK, 1979).
16. P. R. Griffiths and J. A. de Haseth, *Fourier Transform Infrared Spectrometry* (Wiley-Interscience, Hoboken, New Jersey, 2007).
17. A. H. Filler, "Apodization and interpolation in Fourier-transform spectroscopy," J. Opt. Soc. Am. **54**, 762-767 (1964).
18. R. H. Norton and R. Beer, "New apodizing functions for Fourier spectrometry," J. Opt. Soc. Am. **66**, 259-264 (1976); erratum: **67**, 419 (1977), http://www.opticsinfobase.org/abstract.cfm?URI=josa-67-3-419.
19. J. K. Kauppinen, D. J. Moffatt, D. G. Cameron, and H. H. Mantsch, "Noise in Fourier self-deconvolution," Appl. Opt. **20**, 1866-1879 (1981).
20. K. Takada, Y. Inoue, H. Yamada and M. Horiguchi, "Measurement of phase error distributions in silica-based arrayed-waveguide grating multiplexers by using Fourier transform spectroscopy," Electron. Lett. **30**, 1671-1672 (1994).
21. K. Takada, T. Tanaka, M. Abe, T. Yanagisawa, M. Ishii, and K. Okamoto, "Beam-adjustment-free crosstalk reduction in 10GHz-spaced arrayed-waveguide grating via photosensitivity under UV laser irradiation through metal mask," Electron. Lett. **36**, 60-61 (2000).
22. H. Yamada, K. Takada, Y. Inoue, Y. Ohmori, and S. Mitachi, "Statically-phase-compensated 10GHzspaced arrayed-waveguide grating," Electron. Lett. **32**, 1580-1582-61 (1996).
23. B. Solheim, "Spatial Heterodyne Spectroscopy (SHS), Spatial Heterodyne Observations of Water (SHOW)," presented at the 12-th ASSFTS (Atmospheric Science from Space using Fourier Transform Spectrometry) workshop, Quebec City, Canada, 18 May 2005.
24. Y. Lin, G. Shepherd, B. Solheim, M. Shepherd, S. Brown, J. Harlander, and J. Whiteway, "Introduction to spatial heterodyne observations of water (SHOW) project and its instrument development," Proc. XIV Int. TOVS Study Conf., 25-31 May 2005, Beijing, China, 835-843 (2005).
25. G. P. Shepherd, *Spectral Imaging of the Atmosphere* (Academic Press, London, UK, 2002).
26. S. Janz, "Silicon-based waveguide technology for wavelength division multiplexing," in *Silicon Photonics*, L. Pavesi and D. J. Lockwood, eds. (Springer-Verlag, Berlin, 2004).
27. L. Labadie, P. Kern, P. Labeye, E. LeCoarer, C. Vigreux-Bercovici, A. Pradel, J.-E. Broquin, and V. Kirschner, "Technology challenges for space interferometry: the option of mid-infrared integrated optics," Adv. Space Res., in press, available online 20 July 2007, http://dx.doi.org/10.1016/j.asr.2007.07.013.
28. R. A. Soref, S. J. Emelett, and W. R. Buchwald, "Silicon waveguided components for the long-wave infrared region," J. Opt. A: Pure Appl. Opt. **8**, 840–848 (2006).

1. Introduction

Miniature spectrometers are key devices in applications that include fiber optic telecommunication networks, environmental sensing, genomics, health diagnostics, and space instrumentation. In many of these applications, devices with both a large optical throughput, or *étendue*, and a high spectral resolution, are desirable. Planar waveguide spectrometers based on echelle gratings and arrayed waveguide gratings can be designed and fabricated with sub-nanometer spectral resolution and very compact chip sizes [1]. For arrayed waveguide gratings it has been demonstrated that the spectral resolution and compactness can be improved by reducing the width of the spectrally imaged slit, that is the width of the input waveguide in the free propagation region [2]. However, to increase the device *étendue* one can abandon the grating concept altogether and consider spectrometers based on interference.

Compared to the grating spectrometers, interferometer based spectroscopic devices offer significant improvement in the light throughput. The large throughput of the Michelson interferometer was first explained in 1954, [3], and it is know as the *étendue* (or Jacquinot) advantage. Bulk optics Michelson type spectrometers are used in a Fourier-transform configuration with a movable mirror in one of the interferometer arms. By scanning the mirror, an interferogram is generated from which the input spectrum is calculated by Fourier transformation. Beside the *étendue* advantage, an additional benefit of the Fourier-transform spectrometers compared to grating-based devices is the Fellgett multiplex advantage [4, 5], which means that spectral information is measured at all wavelengths simultaneously.

#89497 - $15.00 USD Received 7 Nov 2007; revised 17 Dec 2007; accepted 18 Dec 2007; published 19 Dec 2007

Various static Fourier-transform interferometers which do not require scanning mirrors or other moving parts have been proposed [6]. For example, a bulk optics spatial heterodyne spectrometer (SHS) has been demonstrated where the spectrum is calculated by the Fourier analysis of a stationary interference pattern [7]. The SHS uses a modified Michelson configuration with mirrors replaced by diffraction gratings. Planar waveguide versions of the SHS have also been proposed. The first such device is Fourier transform arrayed waveguide grating (FT-AWG) microspectrometer [8]. In the Fresnel diffraction regime, a FT interleaved AWG device exhibits a distinct interference pattern referred to as the Moiré-Talbot effect [9]. Recently, the waveguide SHS concept has been generalized into a waveguide Mach-Zehnder interferometer (MZI) array [10]. A planar waveguide SHS offers a larger *étendue* compared to arrayed waveguide gratings and waveguide echelle gratings. The SHS can tolerate larger input wavefront angular errors, thus resulting in an increased light throughput [11]. In the arrayed waveguide MZI, the throughput is increased by using multiple input waveguide apertures which feed into an array of Mach-Zehnder interferometers.

In this paper, we follow-up the preliminary results of [10] and present a complete theoretical model and simulations of the arrayed MZI spectrometer. The spectrometer principle is based on the wavelength-dependent transmission characteristics of the individual Mach-Zehnder interferometers and their spatial distribution as the MZI array. We demonstrate the retrieval of input spectrum based on Fourier transformation of spatial light distribution (fringes) at the outputs of the array. Design rules for the required number of interferometers and their respective phase delays are deduced using the sampling theorem. Finally, the device concept and theory are illustrated by a specific design based on silicon-on-insulator waveguides for the application of space-born observation of water transport in the atmosphere in the near infrared spectral region.

2. Principle of multiaperture arrayed Mach-Zehnder interferometer

The Mach-Zehnder interferometer is an established device both in bulk optics and waveguide implementations, with applications including spectral filtering, signal modulation and sensing. It has periodic transmission characteristics which is a function of the phase delay between the two interferometer arms. In static applications the phase delay is typically achieved by making one of the arms longer than the other, thus making the interferometer unbalanced. The optical path difference can be well controlled by the photolithographic processes of waveguide fabrication. Alternatively, a modification of the refractive index in the waveguide arms can be used. For an individual MZI, the frequency of periodic transmission as a function of wavelength increases with the phase delay which means higher wavelength resolution for more unbalanced devices. A picometer resolution has been demonstrated in a highly unbalanced MZI fabricated in silica waveguides [12].

We use the property of periodic MZI transmission to form a new type of spectrometer device. The device is based on an array of independent MZIs with different phase delays as shown schematically in Fig. 1. The device has a multiaperture input formed by N waveguides each feeding into an individual MZI. The spacing between the input waveguides is chosen to ensure that they are optically uncoupled. The input signal propagates through the arrayed MZIs and, as a result of interference, forms a spatially distributed power pattern across their output ports. The output power distribution is measured by a matched photodetector array and digitally processed to retrieve the input spectrum. It is assumed that the input light spectrum does not vary substantially across the multiaperture input, thus all waveguides probe spectrally identical signals, but they do not have to capture identical amount of light. The non-uniformity of light capture among individual MZIs can be calibrated out as described in Sec. 3.3. An obvious advantage of this device is that the optical throughput is largely increased by using multiple inputs simultaneously.

In bulk optics instruments, the throughput (*étendue*) is a geometric factor representing the amount of light captured by the optical instrument. The geometric *étendue* is a product of the source area and the solid angle subtended by the input aperture [13] and it is an invariant of the optical system. The *étendue* of our final spectrometer implementation will depend on

#89497 - $15.00 USD Received 7 Nov 2007; revised 17 Dec 2007; accepted 18 Dec 2007; published 19 Dec 2007

specifics of the input optics and its coupling efficiency to the input waveguides. An optical element that efficiently couples light into the array of input singlemode waveguides can be, for example, a microlens array followed by waveguide tapers feeding into individual MZIs. Another method is using a free propagation region at the input of the waveguide slab followed by tapers, similarly as it is routinely done in the design of waveguide star couplers and AWGs. However, such particulars of the input optics design are out of the scope of this paper, which focuses on MZI array concept and design. It should also be noticed that the concept of geometrical *étendue* does not rigorously apply to waveguide optics since the geometrical optics approximations cease to be valid for the latter. Nonetheless, a simple but still valid *étendue* argument can be made, which is fundamental for our device: throughput increase of this multiaperture device compared to a single aperture device is proportional to the number of waveguide inputs. It thus becomes obvious that the present spectrometer has an advantage compared to single-aperture devices when measuring signals from spatially extended light sources (e.g., the sun) which can be imagined onto an extended multiaperture input.

The operating principle of the device can be understood as follows. The path difference ΔL_i in the MZI array changes by a constant increment across the array. For a given monochromatic input, different transmission characteristics of each MZI results in a different power value at its output. In general, a monochromatic input results in a periodic (sinusoidal) spatial distribution of power across the different output ports $P^{out}(x_i)$, that is the Fourier-transform of the monochromatic input spectrum. Since the spatial power distribution $P^{out}(x_i)$ and the input spectrum are a Fourier transform pair, a polychromatic input produces a power distribution from which the input spectrum can be calculated using Fourier transformation.

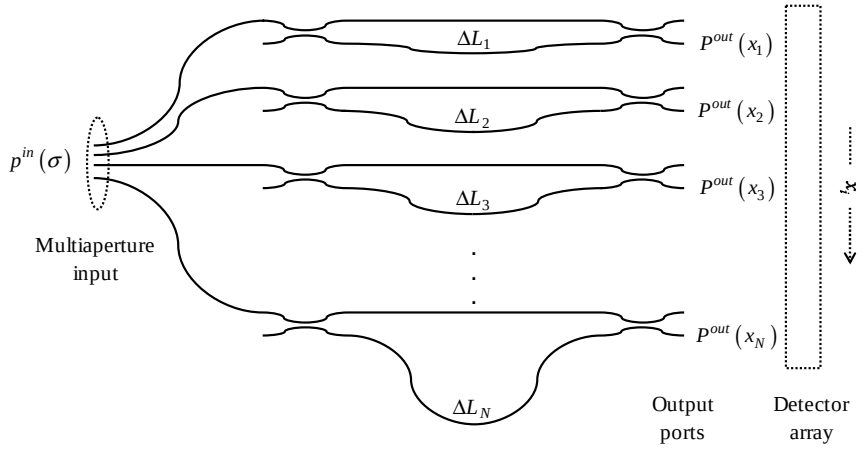

Fig. 1. The schematics of the waveguide spectrometer formed by arrayed Mach-Zehnder interferometers.

Inspecting this device, it is noticed that the MZI array can be designed such that for a particular monochromatic input of a wavenumber $\sigma_L=1/\lambda_L$, a constant spatial power distribution is obtained at the output, as shown in Fig. 2(a). We denote this as the Littrow condition, with the zero spatial frequency corresponding to the Littrow wavenumber σ_L. At the Littrow condition, the phase delays in different MZIs are integer multiples of 2π, thus yielding the constant $P^{out}(x_i)$. As the wavenumber of the monochromatic input σ changes from the Littrow value, the output power distribution becomes periodic with the spatial frequency increasing with $|\sigma-\sigma_L|$. Changing the wavenumber from the Littrow condition to $\sigma_L+\delta\sigma$, where $\delta\sigma$ is the instrument resolution, results in one spatial fringe along the output ports as shown in Fig. 2(b).

#89497 - $15.00 USD Received 7 Nov 2007; revised 17 Dec 2007; accepted 18 Dec 2007; published 19 Dec 2007

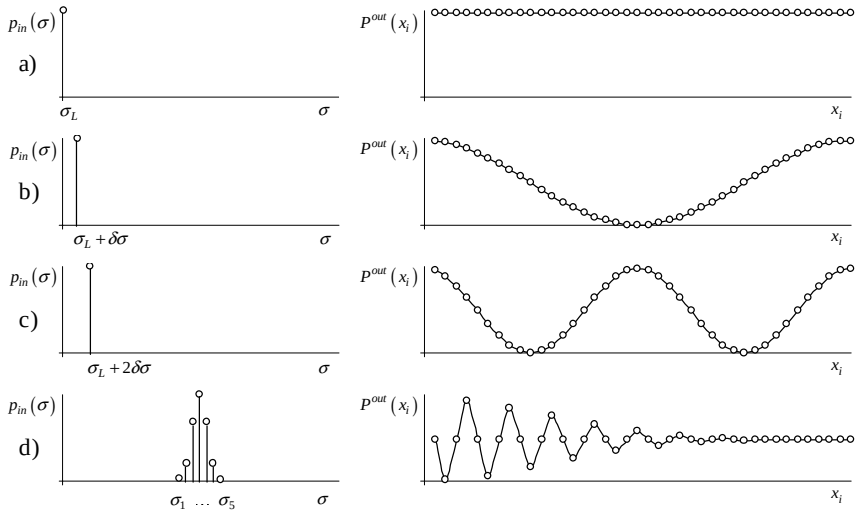

Fig. 2. Spatial fringe formation at the arrayed MZI outputs. Monochromatic inputs at a) the Littrow wavenumber σ_L, b) $\sigma_L+\delta\sigma$, and c) $\sigma_L+2\delta\sigma$, and the corresponding spatial fringes; d) Superposition of monochromatic inputs and the corresponding spatial fringe pattern.

Similarly, the light signal of wavenumber $\sigma_L+2\delta\sigma$ produces two spatial fringes, Fig. 2(c), and so on - monochromatic inputs with different wavenumbers result in different periodic patterns. Since a polychromatic signal can be represented by superposition of monochromatic constituents, a corresponding fringe pattern is formed by superposition of the respective periodic fringes, as illustrated in Fig. 2(d). The parameter $\delta\sigma$ is inversely proportional to the maximum path delay $\Delta L_{\max}$ and is described in the next section.

Wavenumbers that are equally spaced above and below the Littrow value produce the same fringe pattern. To avoid this ambiguity one needs to block one of the two redundant sets of wavenumbers. In the example of Fig. 2 and in calculations presented in Sec 4, the Littrow condition coincides with the minimum wavenumber of the spectral range and wavenumbers below σ_L are assumed to be blocked by a bandpass filter. The spatial fringes can be regarded as single-sided interferograms from which the input spectra can be retrieved assuming the pattern is symmetric with respect to the point of origin (x = 0). We observe that the device heterodynes the spatial interference pattern with respect to the Littrow wavenumber, hence the name spatial heterodyne spectrometer (SHS). The spatial heterodyning in this device has a similar meaning as in the bulk optics SHS instrument [7]. The input spectrum and the output spatial distribution are related through an invertible linear transform which, as argued above and as will be mathematically shown in the next section, is the Fourier cosine transform. It may also be observed that the above principle applies to any arrayed MZI device implementation provided that signal splitting, combining and loss mechanisms in the MZIs can be treated as spectrally independent.

3. Mathematical model

The mathematical model of the arrayed MZI is abstracted from waveguide particulars and can be conveniently described using transfer matrices. The model is first introduced for monochromatic input signals and then generalized to polychromatic light.

3.1 Monochromatic input and transfer matrix formalism

Consider a monochromatic signal propagating in the planar MZI structure and assume that the waveguides support only a fundamental guided mode. The modal electric and magnetic fields

#89497 - $15.00 USD Received 7 Nov 2007; revised 17 Dec 2007; accepted 18 Dec 2007; published 19 Dec 2007

E and **H** can be expressed as products of the complex modal amplitude *a*, the transverse field distributions **e**(*x*, *y*) and **h**(*x*, *y*), and the exponential propagation factor

$$\mathbf{E}(x,y,z,t) = a\,\mathbf{e}(x,y)e^{i(\omega t-\beta z)} \qquad \mathbf{H}(x,y,z,t) = a\,\mathbf{h}(x,y)e^{i(\omega t-\beta z)} \tag{1}$$

where $\beta = kn_{eff} = 2\pi\sigma n_{eff}$ is the mode propagation constant, $\sigma = 1/\lambda$ is the wavenumber, and n_{eff} is the effective mode index. The monochromatic modal power *P* is given by the Poynting vector

$$P = \frac{1}{2}|a|^2 \iint \mathbf{e}\times\mathbf{h}^* \cdot \hat{\mathbf{z}}\,dxdy \tag{2}$$

where the integration is over the transverse plane (*x*, *y*) containing the waveguide cross-section and the asterisk indicates the complex conjugate.

A generic Mach-Zehnder interferometer can be represented in terms of three functional sections which perform signal splitting, provide a differential phase delay, and recombine the two split signals, respectively. Now we assume that the waveguides, the splitters and the combiners are polarization independent (polarization effects will be discussed in Section 3.5). It is convenient to represent the propagation of the light signal in each MZI by using discrete transformations of the modal amplitude *a* along the two waveguide paths, i.e. in the lower and upper arms and the corresponding ports of the MZI structure. This can be done by using the transfer matrix formalism [14]. In their feed-forward implementation, the transfer matrices are equivalent to scattering matrices, thus the two terms may be used interchangeably. The transfer matrix notation used here is illustrated in Fig. 3.

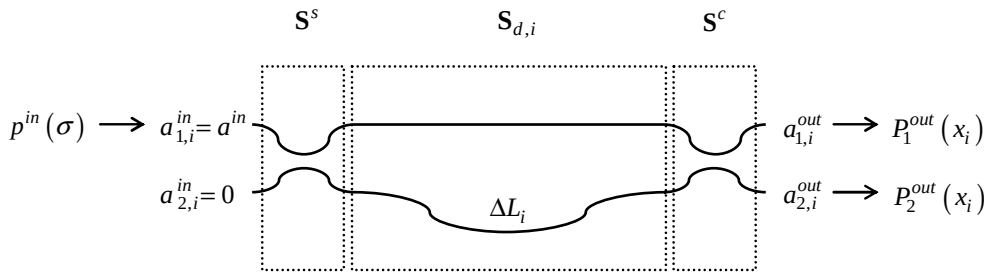

Fig. 3. Transfer matrix notation used in the model.

The transfer matrix model represents each MZI as a device with two input and two output ports. The optical signal propagating in the *i*-th MZI is represented by a column vector with modal amplitudes $a_{1,i}$ and $a_{2,i}$ which correspond to the two different waveguide arms and the corresponding ports. It is assumed that the main difference between the MZIs is in their delay sections. The functional sections of the *i*-th MZI are described by three 2×2 transfer matrices $\mathbf{S}_s$, $\mathbf{S}_d$, and $\mathbf{S}_c$ representing amplitude transfers in the splitter, the delay section, and the combiner, respectively. Each MZI of the array is then described by the cumulative transfer matrix $\mathbf{S}_i$ which is a product of the three section matrices

$$\begin{bmatrix} a_{1,i}^{out} \\ a_{2,i}^{out} \end{bmatrix} = \mathbf{S}_i \cdot \begin{bmatrix} a_{1,i}^{in} \\ a_{2,i}^{in} \end{bmatrix} = \mathbf{S}_c \cdot \mathbf{S}_{d,i} \cdot \mathbf{S}_s \cdot \begin{bmatrix} a_{1,i}^{in} \\ a_{2,i}^{in} \end{bmatrix} \tag{3}$$

Since waveguide details are embedded in the matrix coefficients, the cumulative matrix $\mathbf{S}_i$ encompasses many practical waveguide designs. However, care should be exercised while assigning the input and output amplitudes and in interpreting simulation results. This is because splitting and combining functions can be realized by different components, e.g., y-junctions, directional couplers, or multimode interference couplers that can be perceived as

#89497 - $15.00 USD Received 7 Nov 2007; revised 17 Dec 2007; accepted 18 Dec 2007; published 19 Dec 2007

three- or four-port devices. In splitters, one assumes that the column vector of the input signal has only one non-zero component $a_{1,i}$ or $a_{2,i}$. In combiners, the interpretation of the output vector depends on the number of output waveguide ports. Combiners based on directional couplers have two output ports that provide complementary signals, while in a y-junction combiner there is only one guided output. Nonetheless, all practical implementations can be cast into the matrix notation above. For clarity, this discussion assumes an implementation with splitters and combiners made of directional couplers. In this case, all Mach-Zehnder sections are represented by transfer matrices that have straightforward interpretation. Designs based on other types of splitters and combiners can be described analogously.

Output directional couplers provide two complementary signals from each MZI and are denoted in Fig. 3 as $P_1^{out}(x_i)$ (upper arm) and $P_2^{out}(x_i)$ (lower arm); however, only one of them is necessary to retrieve the input spectrum. Accordingly, in Fig. 1 the symbol $P^{out}(x_i)$ refers to the output of the lower arm. In Sec. 3.3, we will discuss how measuring both these complementary signals can be used for power calibration and apodization.

Transfer matrices of the directional couplers for splitting and combining, $\mathbf{S}_s$ and $\mathbf{S}_c$ are similar. They can be expressed in terms of a product of the respective power transmission factors γ_s and γ_c, and mode coupling matrices which contain the power coupling ratios κ_s and κ_c, that is

$$\mathbf{S}_s = \gamma_s \begin{bmatrix} \sqrt{1-\kappa_s} & -i\sqrt{\kappa_s} \\ -i\sqrt{\kappa_s} & \sqrt{1-\kappa_s} \end{bmatrix} \qquad \mathbf{S}_c = \gamma_c \begin{bmatrix} \sqrt{1-\kappa_c} & -i\sqrt{\kappa_c} \\ -i\sqrt{\kappa_c} & \sqrt{1-\kappa_c} \end{bmatrix} \tag{4}$$

It is observed that for a lossless operation $\gamma_s = \gamma_c = 1$, and for equal splitting and combining of power $\kappa_s = \kappa_c = 1/2$.

We introduce waveguide loss in terms of the linear propagation loss coefficient α and assume that the i-th MZI delay section is formed by two waveguides of lengths $L_{1,i}$ and $L_{2,i}$ where $L_{2,i} > L_{1,i}$. The transfer matrix of the delay section is a product of the transmission factor $\gamma_{d,i} = \exp(-\alpha L_{2,i})$ and the phase factor $\exp(-\beta L_{2,i})$ through the common path length, and the delay matrix of the differential path $\Delta L_i = L_{2,i} - L_{1,i}$

$$\mathbf{S}_{d,i} = \gamma_{d,i} e^{-i\beta L_{2,i}} \begin{bmatrix} e^{-\alpha\Delta L_i} e^{-i\beta\Delta L_i} & 0 \\ 0 & 1 \end{bmatrix} \tag{5}$$

The delay matrix contains the differential loss factor $\alpha\Delta L_i$ which is usually small and may be ignored. For each MZI, we assume that the same input signal of modal power $P^{in} = |a^{in}|^2$ is present at the input port 1 and that the input port 2 is not used, as indicated in Fig. 3. Using the transfer matrix method, the powers at the output ports 1 and 2 of the i-th MZI are then

$$P_1^{out}(x_i) = P_{1,i}^{out} = \frac{1}{2} P^{in} \left[A_{1,i} - B_i \cos\beta\Delta L_i \right] \tag{6}$$

$$P_2^{out}(x_i) = P_{2,i}^{out} = \frac{1}{2} P^{in} \left[A_{2,i} + B_i \cos\beta\Delta L_i \right] \tag{7}$$

In both ports, the detected signal consists of a fluctuating part given by cosinusoidal variation and a constant background. The coefficients $A_{1,i}$, $A_{2,i}$, and B_i comprise the coupling and loss coefficients of the MZI components and are given by the following expressions

$$A_{1,i} = 2\gamma_s^2 \gamma_{d,i}^2 \gamma_c^2 \left[\kappa_s \kappa_c + (1-\kappa_s)(1-\kappa_c) e^{-2\alpha\Delta L_i} \right] \tag{8}$$

$$A_{2,i} = 2\gamma_s^2 \gamma_{d,i}^2 \gamma_c^2 \left[\kappa_s (1-\kappa_c) + \kappa_c (1-\kappa_s) e^{-2\alpha\Delta L_i} \right] \tag{9}$$

#89497 - $15.00 USD Received 7 Nov 2007; revised 17 Dec 2007; accepted 18 Dec 2007; published 19 Dec 2007

$$B_i = 4\gamma_s^2\gamma_{d,i}^2\gamma_c^2\left[\kappa_s\kappa_c\left(1-\kappa_s\right)\left(1-\kappa_c\right)\right]^{\frac{1}{2}} e^{-\alpha\Delta L_i} \tag{10}$$

The above coefficients are real valued numbers which can be determined experimentally. For a lossless case with equal 50:50 splitting and combining we have $A_{1,i} = A_{2,i} = B_i = 1$. In that case Eqs. (6, 7) represent ideal interference of two monochromatic signals.

3.2 Polychromatic input and Fourier transformation

For the light spectrum consisting of discrete monochromatic constituents, the output power can be represented by a sum of the contributing signals each corresponding to a specific monochromatic input. For sources with a continuous spectral distribution, it is convenient to introduce the spectral power $p(\sigma)$ (spectral flux, lower case symbol), which is the power within a small range of wavenumbers from σ to $\sigma + d\sigma$. From the superposition principle, the interferometric expressions for the output powers corresponding to Eqs. (6, 7) are given by the following integral equations

$$\int_0^\infty p_{1,i}^{out}\left(\sigma\right)d\sigma = \frac{1}{2}\int_0^\infty p^{in}\left(\sigma\right)\left[A_{1,i} - B_i\cos\left(2\pi\sigma n_{\text{eff}}\Delta L_i\right)\right]d\sigma \tag{11}$$

$$\int_0^\infty p_{2,i}^{out}\left(\sigma\right)d\sigma = \frac{1}{2}\int_0^\infty p^{in}\left(\sigma\right)\left[A_{2,i} + B_i\cos\left(2\pi\sigma n_{\text{eff}}\Delta L_i\right)\right]d\sigma \tag{12}$$

The integration here assumes that the optical power is measured by a detector with a bandwidth broader than the spectral width of the input signal. A spectral responsivity function of the detector can be readily included in the integrals above. However, to simplify the notation we assume an ideal broadband detector with a flat spectral response. In many practical cases, including the application example of Sec. 4 below, the coefficients $A_{1,i}$, $A_{2,i}$, and B_i can be regarded as wavelength independent in the spectral range of interest. With this assumption, the interference formulas Eqs. (11, 12) are simplified to

$$P_{1,i}^{out} = \frac{1}{2}A_{1,i}P^{in} - \frac{1}{2}B_i\int_0^\infty p^{in}\left(\sigma\right)\cos\left(2\pi\sigma n_{\text{eff}}\Delta L_i\right)d\sigma \tag{13}$$

$$P_{2,i}^{out} = \frac{1}{2}A_{2,i}P^{in} + \frac{1}{2}B_i\int_0^\infty p^{in}\left(\sigma\right)\cos\left(2\pi\sigma n_{\text{eff}}\Delta L_i\right)d\sigma \tag{14}$$

where P^{in}, $P_{1,i}{}^{out}$, and $P_{2,i}{}^{out}$ are the measured powers (upper case symbols), i.e. the respective spectral fluxes integrated by the detector. These formulas can be further simplified by introducing the following interference term

$$F_i = -\frac{1}{B_i}\left(2P_{1,i}^{out} - A_{1,i}P^{in}\right) = \frac{1}{B_i}\left(2P_{2,i}^{out} - A_{2,i}P^{in}\right) \tag{15}$$

The interference term $F_i = F(x_i)$ is a modified spatial interferogram which in normal device operation will be created in the signal processing step based on measured powers. The spatial coordinate x_i is measured in units of ΔL_i, so we set it equal to the optical path difference $x_i = n_{eff}\Delta L_i$ and call it the modified delay. Consequently, on a physical waveguide layout, the discrete output ports need not be uniformly distributed as long as the MZI delay increment is constant and the output port readings are digitally processed in the same increasing order.

One can formally demonstrate an analogy with the standard Fourier-transform spectrometry and consider very small delay increments and a large number of MZI, thus reaching a continuous limit in the formulas. From Eqs. (13-15) the continuous limit

#89497 - $15.00 USD Received 7 Nov 2007; revised 17 Dec 2007; accepted 18 Dec 2007; published 19 Dec 2007

interferogram and the input spectral power $p^{in}(\sigma)$ are related through the Fourier cosine transform

$$F(x) = \int_0^\infty p^{in}(\sigma)\cos 2\pi\sigma x \, d\sigma = \int_{-\infty}^{\infty} p^{in}(\bar{\sigma})\cos 2\pi\bar{\sigma}x \, d\bar{\sigma} \tag{16}$$

In the last equation we introduced the shifted wavenumber variable $\bar{\sigma} = \sigma - \sigma_{\min}$, where $\sigma_{\min}$ is a minimum wavenumber. Since we are interested in a limited spectral range $\Delta\sigma = \sigma_{\max} - \sigma_{\min}$ outside which the spectral power vanishes, one may extend the lower integration limit in the last equation to infinity. In the present design, the minimum wavenumber is the Littrow wavenumber. An identical expression to Eq. (16) is obtained for an interferogram produced at the output of an ideal two-beam free-space interferometer with a variable path delay x irradiated by the power spectrum $p^{in}(\sigma)$ [15, 16]. Assuming that the interferogram $F(x)$ is symmetric with respect to $x = 0$, the inverse relation holds

$$p^{in}(\bar{\sigma}) = \int_{-\infty}^{\infty} F(x)\cos 2\pi\bar{\sigma}x \, dx = 2\int_0^\infty F(x)\cos 2\pi\bar{\sigma}x \, dx \tag{17}$$

This cosine transform is the fundamental relation in the Fourier transform spectrometry, including our arrayed MZI spectrometer. It allows one to retrieve the input spectrum $p^{in}(\sigma)$ from the measured interferogram $F(x)$.

3.3 Interferogram discretization and apodization

In practical waveguide device implementations, the spatial interferogram $F(x_i)$ is discretized at N equally spaced delay values x_i ($0 \le x_i \le \Delta x$) corresponding to the outputs of different MZIs, where the maximum delay is Δx. By analogy to the integral formula Eq. (17), the input spectrum is calculated from the measured interferogram using the following discrete Fourier cosine transform

$$p^{in}(\bar{\sigma}) = \frac{\Delta x}{N} P^{in} + 2\frac{\Delta x}{N}\sum_{i=1}^{N} F(x_i)\cos 2\pi\bar{\sigma}x_i \tag{18}$$

where the interferogram $F(x_i)$ is defined in Eq. (15) from $P_1^{out}(x_i)$ or $P_2^{out}(x_i)$. Using Eqs. (15) and (18) the input spectrum can be then calculated from the measured powers.

For a uniform illumination of the multiaperture input, the input modal power P^{in} is constant for all the input waveguides ($P^{in}_i = P^{in}$). For a non-uniform illumination, P^{in}_i can be measured directly with a probing waveguide or, alternatively, one can use the complementary output powers $P_1^{out}(x_i)$ and $P_2^{out}(x_i)$ to calculate P^{in}_i from

$$P_i^{in} = 2\left(P_{1,i}^{out} + P_{2,i}^{out}\right) / \left(A_{1,i} + A_{2,i}\right) \tag{19}$$

which is obtained from Eqs. (6) and (7). Thus, by measuring $P_1^{out}(x_i)$ and $P_2^{out}(x_i)$ at the complementary output ports the input modal power is obtained for each MZI. Eq. (19) can be readily applied to correct for spatial non-uniformities in the input beam using software calibration. In this procedure the inverse Fourier formula Eq. (18) is used with $P^{in} = \max(P^{in}_i)$ and the interferogram F_i is multiplied by the ratio $c_i = P^{in}/P^{in}_i$.

By analogy to the continuous Fourier-transform spectrometry the finite summation in Eq. (18) corresponds to a step-like cut-off (truncation) in the spatial interferogram distribution [15]. It is known that such truncation causes oscillatory features (ripple) in the retrieved spectrum. The ripple can be reduced by apodization. For this purpose, we apodize the interferogram by using the weighting function $W(x)$, thus obtaining the following spectrum retrieval formula

#89497 - $15.00 USD Received 7 Nov 2007; revised 17 Dec 2007; accepted 18 Dec 2007; published 19 Dec 2007

$$p^{in}(\bar{\sigma}) = \frac{\Delta x}{N} P^{in} + 2\frac{\Delta x}{N}\sum_{i=1}^{N} W(x_i)F(x_i)\cos 2\pi\bar{\sigma}x_i \tag{20}$$

Many suitable apodization functions are known in the field of Fourier spectrometry [17-19]. We recall that in the above discussion it was assumed that the device coefficients $A_{1,i}$, $A_{2,i}$, and B_i do not vary between different MZIs. By inspecting Eqs.(15) and (20) we see that this assumption is not a restricting one, since variations in the coefficients (including propagation loss) can be formally included in the apodization function.

3.4 Design rules for maximum path delay and minimum number of interferometers

The wavenumber resolution $\delta\sigma$ of the spectrometer is determined by the maximum interferometric delay Δx, that is the delay corresponding to the most unbalanced MZI in the array. To resolve two monochromatic signals with wavenumbers σ and $\sigma + \delta\sigma$ it is required that the respective interferograms differ by one fringe, that is, an interferogram phase change of 2π

$$\Delta\varphi = 2\pi(\sigma + \delta\sigma)\Delta x - 2\pi\sigma\Delta x = 2\pi \tag{21}$$

thus $\delta\sigma\Delta x = \delta\sigma n_{eff}\Delta L_{max} = 1$. This can also be represented using the wavelength resolution $\delta\lambda$ near the central wavelength of the range λ_0, where $\delta\lambda \ll \lambda_0$. A useful expression for ΔL_{max} can be obtained in terms of the resolving power $R = \lambda_0/\delta\lambda$ which is often used in grating spectroscopic devices

$$\delta\sigma = \frac{1}{\lambda_0} - \frac{1}{\lambda_0 + \delta\lambda} \approx \frac{\delta\lambda}{\lambda_0^2} = \frac{1}{R}\frac{1}{\lambda_0} \tag{22}$$

The maximum path delay of the arrayed MZI is thus

$$\Delta L_{max} = \frac{1}{\delta\sigma n_{eff}} = R\frac{\lambda_0}{n_{eff}} \tag{23}$$

The number of discrete points N in the interferogram, that is the number of MZIs in the array, is determined from the Fourier sampling theorem. According to the theorem, for the spectral power non-vanishing only within the range $\Delta\sigma$, the spectrum $p^{in}(\sigma)$ is fully specified by sampling the interferogram at spectral intervals not exceeding $(2\Delta\sigma)^{-1}$. In other words, the minimum number of sampling points is

$$N_{min} = 2\Delta x\Delta\sigma = 2\frac{\Delta\sigma}{\delta\sigma} = 2\frac{\Delta\lambda}{\delta\lambda} \tag{24}$$

where $\Delta\lambda$ is the wavelength spectral range of the spectrometer. For example, an arrayed MZI spectrometer operating over the 2.5 nm wavelength range at 0.1 nm resolution requires 50 MZIs. Since each MZI couples to a separate input waveguide, in this example the optical throughput is increased by a factor of 50 compared to a single input device.

The discrete Fourier transform formulas Eqs. (18, 20) with the criteria for maximum delay Eq. (23) and the number of sampling points (interferometers) Eq. (24) constitute a closed model of the arrayed Mach-Zehnder spectrometer. The measurement required to be physically performed by the interferometer is that of the optical power values at the multiple outputs of the array. Performance details of various waveguide components are contained in coupling and loss coefficients given by Eqs. (8-10). These can be measured independently and their values introduced into the calculations as constant device parameters. Deviations from the ideal design will appear as systematic errors in the interferograms. Once the waveguide device has been fabricated and characterized, the errors can be eliminated by a calibration procedure, for example using a look-up table incorporated in the retrieval algorithm. That calibration ability is an important advantage of the present device compared

#89497 - $15.00 USD Received 7 Nov 2007; revised 17 Dec 2007; accepted 18 Dec 2007; published 19 Dec 2007

to conventional AWGs. Since in the AWGs there is no direct physical access to the arrayed waveguide output aperture, measuring and correcting phase errors of an AWG is a formidable task. It demands sophisticated phase measurement techniques like low coherence interferometry [20]. That is followed by complex phase correction techniques by UV exposure through two masks, one for transverse electric (TE) and one for transverse magnetic (TM) polarization [21], or by depositing an amorphous-Si mask and trimming it by laser ablation [22]. In contrast to the AWGs, our device provides physical access to each of the arrayed MZI outputs where both phase and amplitude errors can be readily measured as part of the spectrometer calibration procedure. It may also be appreciated that complementary signals from the output ports 1 and 2 of each MZI may be used for additional corrections of spatial non-uniformity of the input beam across the multiple aperture.

3.5 Polarization dependence

Since in many applications the polarization state of the input light is not known, polarization independent spectrometer design is preferred. Polarization changes of light would cause the measured wavenumber to change by $\delta\sigma_{pol}$ due to waveguide birefringence Δn_{eff}, thus causing uncertainty in the spectral measurement. The physical origin of this effect is well understood [1]. If the MZI waveguides are birefringent, orthogonally polarized modes propagate with different propagation constants, thus accumulating differential phase shifts in the two interferometer arms. The birefringence induced phase shift is indistinguishable from the one that would arise if the input light wavelength were changed. Thus, to avoid a false spectral interpretation birefringence needs to be mitigated. At the center of the measured spectral range σ_0 the phase change caused by waveguide birefringence in any MZI is $\Delta\varphi_i = 2\pi\Delta n_{eff}\Delta L_i\sigma_0$. The polarization dependent wavenumber shift $\delta\sigma_{\mathrm{pol}}$ can be formally estimated by equaling the birefringence induced phase change with the phase change caused by the wavenumber shift at the average effective index, that is $\Delta\varphi_i = 2\pi n_{eff}\Delta L_i\delta\sigma_{pol}$. Therefore, the spectral uncertainty induced by the waveguide birefringence is

$$\delta\sigma_{pol} / \sigma_0 \approx \delta\lambda_{pol} / \lambda_0 = \Delta n_{neff} / n_{neff} \tag{25}$$

where $\delta\sigma_{pol} \ll \sigma_0$. The above relation is well-known in the field of echelle and arrayed waveguide grating (de)multiplexers [1].

4. Arrayed MZI implementation for water vapor spectroscopy in near infrared

A design model of the arrayed MZI spectrometer has been developed for the application in spatial heterodyne observations of water (SHOW) [23]. The arrayed MZI spectrometer can be regarded as a integrated waveguide counterpart of the bulk optics SHOW instrument designed for measurements of water vapor transport from the upper atmosphere through the stratosphere and into the lower mesosphere by observing sunlight in limb configuration [24, 25]. SHOW experiments include detection of water absorption bands on the solar irradiance background in the 2 nm wavelength range centered at 1364.5 nm, with spectral resolution 0.1 nm. For such narrow spectral range, material and waveguide dispersion is assumed to be negligible.

In the SHOW example presented here, the light at the spectrometer input has the spectral power distribution of water vapor at the altitude 15 km, as shown in Fig. 4. This transmission spectrum was obtained by using the pseudo-spherical multiple scattering radiative transfer model LIMBTRAN, where temperature, pressure and H_2O profiles were used with the Canadian Middle Atmosphere Model (CMAM) and line strengths were from the HITRAN 2004 database for high-resolution transmission molecular absorption [23].

#89497 - $15.00 USD Received 7 Nov 2007; revised 17 Dec 2007; accepted 18 Dec 2007; published 19 Dec 2007

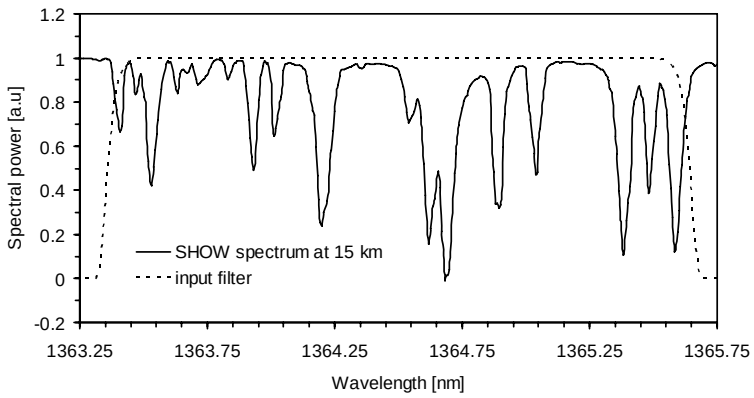

Fig. 4. Transmission spectra of water vapor at 15 km altitude. The bandpass input filter spectrum is also shown.

It is assumed that the signal input to the arrayed MZI is limited by a bandpass filter which attenuates all wavelengths beyond the spectral range $\Delta\lambda$ = 2.5 nm, as showed by the dashed line in Fig. 4. The filter has a super-Gaussian transmission that is nearly flat within the 2 nm spectral range of interest (1363.5 – 1365.5 nm).

The arrayed MZI spectrometer is simulated for the silicon-on-insulator (SOI) waveguide platform. The SOI structure comprises a top single crystal Si layer acting as a waveguide core separated from the Si wafer by a thin SiO_2 bottom cladding layer [26]. In our implementation we assume ridge waveguides formed by partially etching the Si layer in the lateral regions and the top cladding is SiO_2. We performed numerical calculations to determine the waveguide cross-sectional dimensions required for the singlemode condition, low bending radiation loss, and zero-birefringence. We choose an SOI with a comparatively thick Si layer (4 μm) to maximize the aperture of the individual waveguides at the chip input edge. According to vectorial mode solver calculations for this SOI thickness, the etch depth of 2.3 μm and the ridge width of 2.6 μm give a singlemode waveguide with the effective index n_{eff} = 3.49769, where the TE and TM polarization modes are degenerate. The minimum bending radius (bend loss < 0.01 dB per 90-degree turn) is 5 mm. According to Eqs. (23, 24), for the wavelength resolution of $\delta\lambda$ = 0.1 nm, an array comprising 50 MZIs with the maximum delay $\Delta L_{\max}$ = 5.3232 mm is required. The MZIs are implemented with s-bend curved waveguides of varying dimensions compliant with the calculated minimum bend radius. The minimum spacing between the uncoupled input waveguides is 20 μm (core-to-core). The overall size of the layout is 3×4 cm^2.

The simulations are performed as follows. The ideal input spectral power $p^{in}(\sigma)$ is defined by the filter limited SHOW spectrum of Fig. 4. The measured input power P^{in} is simulated by numerical integration of $p^{in}(\sigma)$ over the spectral range. The measured output powers $P_{1,i}^{out}$ and $P_{2,i}^{out}$ are calculated for each MZI based on Eqs. (13, 14) with its respective coefficients defined by Eqs. (8-10). In the following steps, the spectral retrieval method is applied. The modified spatial fringe pattern is calculated from Eq. (15) and the apodized spectrum is obtained from the fringe pattern using the spectral retrieval formula Eq. (20). The simulation results are shown in Fig. 5.

#89497 - $15.00 USD Received 7 Nov 2007; revised 17 Dec 2007; accepted 18 Dec 2007; published 19 Dec 2007

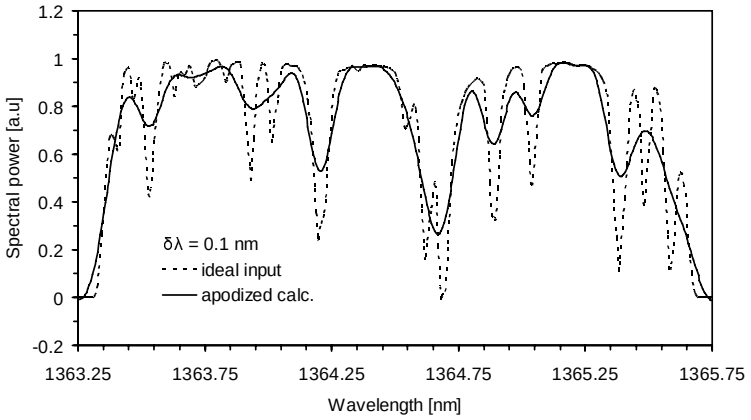

Fig. 5. Ideal input and apodized calculated spectra for the arrayed MZI spectrometer with 0.1 nm resolution.

In the spectral calculations the following apodization function was used

$$W(x_i) = \left[1 - \left(\frac{x_i}{x_{max}}\right)^2\right]^2 = \left[1 - \left(\frac{\Delta L_i}{\Delta L_{max}}\right)^2\right]^2 \tag{26}$$

By comparing the calculated and the ideal spectra in Fig. 5 it is observed that some spectral features are lost, for example a double minimum in the vicinity of 1364.65 nm. This is because features finer than the Rayleigh resolution limit (0.1 nm) cannot be resolved. These spectral features can be retrieved by improving the spectrometer resolution from 0.1 nm to 0.025 nm. This is done by increasing the maximum delay from 5.32 mm to 21 mm and using 200 MZI structures instead of 50. It is noticed that the optical throughput of such device is increased by a factor of 200 compared to a single aperture device. The calculated spectrum is shown in Fig. 6 with most of the spectral features of the ideal input being correctly retrieved.

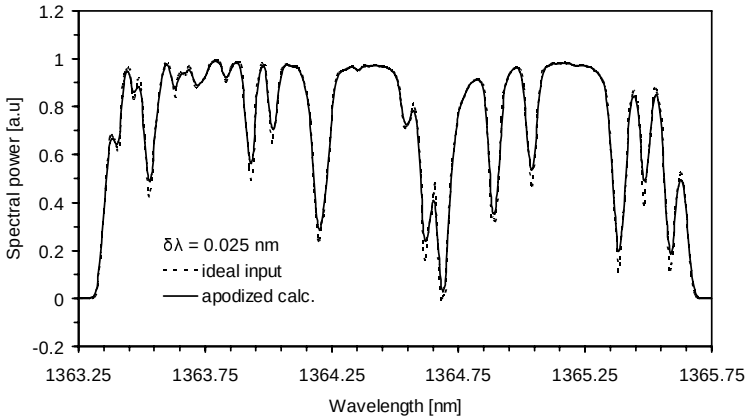

Fig. 6. Ideal input and apodized calculated spectra for the arrayed MZI spectrometer with 0.025 nm resolution.

#89497 - $15.00 USD Received 7 Nov 2007; revised 17 Dec 2007; accepted 18 Dec 2007; published 19 Dec 2007

Due to the comparatively large number of MZI structures and the maximum phase delay required, the last design example poses a challenge if low index contrast planar waveguides are used, however it can be readily implemented in high index contrast (HIC) waveguides such as SOI or silicon oxynitride, the latter also extending the device spectral transparency to the visible range. The size of the device depends on the minimum bending radius of the waveguide platform used. For example, using silicon wire waveguides with the 10 um bending radius would result in a SHOW spectrometer with a footprint of a few square millimeters.

Assuming that the appropriate waveguides are available the arrayed MZIs can be used for spectrometry and sensing beyond the near-infrared and visible spectral regions. In the mid-infrared region, waveguides have been developed for nulling interferometry, where different types of waveguide technologies have been studied for application in the 6-20 μm range of the DARWIN space project [27]. These include chalcogenide glass, ZnSe/ZnS, and metallic hollow waveguides. Silicon technology may also be extended to the long-wave infrared region by using Si rib membrane, germanium-on-silicon, and Si-based hollow-core waveguides [28]. Implementation of arrayed MZI spectrometers using these waveguides will depend on the precise knowledge of mode properties, the minimum bending radius, and design details of splitters and combiners, although the general model of Sec.3 still applies for their design.

5. Conclusions

The main advantages of the proposed arrayed waveguide Mach-Zehnder spectrometer are a large optical throughput and a compact and static (no moving parts) design. The latter is a unique feature of Fourier-transform SHS spectrometers. These are important benefits in applications where size and weight are critical, for example in hand-held spectroscopic instrumentation or deployment on micro- and nano-satellites. Last, but not least, fabrication robustness is an important advantage of the arrayed MZI compared to the state-of-the-art echelle and arrayed waveguide grating technologies. This is because phase and amplitude errors can be readily measured and corrected by calibration software with no need for costly modification of the waveguide physical properties by microfabrication tools. Apodization can also be implemented in calibration software obviating the need for dedicated apodizing optical elements.

Acknowledgments

This work was supported by the Canadian Space Agency, COM DEV Ltd., and the National Research Council Canada, through the project “Slab waveguide spatial heterodyne spectrometer”, CSA 9F028-064201/007/MTB.

#89497 - $15.00 USD Received 7 Nov 2007; revised 17 Dec 2007; accepted 18 Dec 2007; published 19 Dec 2007